CCI

BIOMASS

NEW SENSORS

VERSION 1.0

DOCUMENT REF:	CCI_BIOMASS_NEWSENSORS_V1
DELIVERABLE REF:	OP2_NEWSENSORS
VERSION:	1.0
CREATION DATE:	2026-03-09
LAST MODIFIED	2026-03-13

Document Authorship

	NAME	FUNCTION	ORGANISATION	SIGNATURE	DATE
PREPARED	M. Santoro	OP2-Lead	GAMMA RS		
PREPARED	H. Balzter	OP2_Co-Lead	University of Leicester		
PREPARED	N. Acil	Research Associate	University of Leicester		
PREPARED	S. Ashgzaran	Research Assistant	University of Leicester		
PREPARED					
PREPARED					
PREPARED					
VERIFIED	S. Quegan	Science Leader	Sheffield University		
VERIFIED	R. Lucas	Project Manager	Aberystwyth University		
VERIFIED	N. Carvalhais	Science Leader	Max Planck Institute		
VERIFIED	A. Harris	Project Coordinator	Aberystwyth University		
APPROVED					

Document Distribution

ORGANISATION	NAME	QUANTITY
ESA	Clement Albergel	

Document History

VERSION	DATE	DESCRIPTION	APPROVED
0.1	2026-03-09	First draft version	
1.0	2026-05-06	Finalised version of deliverable	

Document Change Record (from Year 1 to Year 2)

VERSION	DATE	DESCRIPTION	APPROVED

TABLE OF CONTENTS

LIST OF FIGURES

LIST OF TABLES

SYMBOLS AND ACRONYMS

AGB	Above Ground Biomass
CCI	Climate Change Initiative
ECV	Essential Climate Variable
ESA	European Space Agency
GCOS	Global Carbon Observing System
ISRO	Indian Space Research Organisation
LiDAR	Light Detection and Ranging
NASA	National Aeronautics and Space Administration
NISAR	NASA-ISRO Synthetic Aperture Radar
SAR	Synthetic Aperture Radar
SNAP	Sentinel Application Platform
UAV	Unmanned Aerial Vehicle

REFERENCE DOCUMENTS

ID	TITLE	ISSUE	DATE
RD-1	Algorithm Theoretical Basis Document	V7	

Introduction

The aim of the European Space Agency (ESA) Climate Change Initiative (CCI) Programme is to advance scientific understanding of the climate system and climate change by producing long-term datasets that meet climate data quality conditions (IPCC, 2003) and that can be readily linked to climate models. A basic input to this process is the series of reports by the Global Carbon Observing System (GCOS) that set out a continually reviewed set of Essential Climate Variables (ECVs) and a process to implement the acquisition of these ECVs.

ESA's BIOMASS and National Aeronautics and Space Administration (NASA)/ Indian Space Research Organisation's (ISRO) NISAR missions carry onboard Synthetic Aperture Radar (SAR) sensors that provide new P- and S-band and ongoing L-band capacity to retrieve AGB from regional to global levels. The P-band frequency of the BIOMASS SAR offers a much-enhanced capability to penetrate even very dense vegetation canopies and to sense their 3-dimensional structure.

The BIOMASS mission was launched on 29 April 2025 and is designed to operate for five years. It carries a fully polarimetric P-band SAR operating at a centre frequency of 435 MHz (70-cm wavelength) with a bandwidth of 6 MHz in Stripmap mode (Quegan *et al.*, 2019). Accordingly, the spatial resolution in the ground range direction is 59 m while the spatial resolution in the azimuth direction is 8 m. Other system performance parameters of interest in this context are the Noise Equivalent Sigma Zero (NESZ) ≤ 30.4 dB, the radiometric stability ≤ 0.26 dB, the geolocation accuracy ≤ 4.1 m and the dynamic range between –30 dB and 5 dB (all predicted).

Wall-to-wall coverage is achieved by imaging three adjacent swaths along a given orbit. Each swath is approximately 50 km wide, with incidence angles varying from 26° to 32° at mid-swath. Although the objective of the mission is to cover forest areas between 75°N and 60°S, interference with the United States Department of Defense Space Object Tracking Radar (SOTR) radars limits the use of the BIOMASS sensor over North America and Europe (see https://earth.esa.int/eogateway/missions/biomass/description). As a result of this limitation, the mission is operated with an operation mask.

BIOMASS started acquiring images in June 2025 and gathered a large number of observations necessary for its calibration during the In-Orbit Commissioning phase. On 21 November 2025, the routine operations started with the tomographic phase. This will last approximately 16 months during which each point within the acquisition mask will be imaged 7 times with a 3-day repeat-interval and a certain spatial baseline optimized to derive accurate vertical profiles of the forest. The interferometric phase will follow and acquire three observations for any location within the acquisition mask.

Data from the calibration and validation phase (CalVal) are currently accessible by a restricted number of users engaged in the calibration/validation activities. Images acquired during the tomographic phase have been available to the public since January 2026. Table 1 lists the different processing levels of BIOMASS data. For details, see https://earth.esa.int/eogateway/missions/biomass/biomass-data.

Table 1. Levels of the BIOMASS data products.

Product level	Product name
L0	Raw data (not public)
L1a	Single-look Complex Slant-range (SCS)

L1b	Detected Ground-range Multi-looked (DGM)
L1c	Stack of coregistered SCS (used for tomography and interferometry) (STA)
L2a	Stack-based biophysical products (forest disturbance, forest height and ground notch)
L2b	Tile-based biophysical products (forest disturbance, forest height and above ground biomass density)
L3	Consolidated global biophysical parameters (forest disturbance, forest height, above ground biomass density)

The NISAR mission (Rosen *et al.*, 2025) is a joint NASA-ISRO satellite mission and was launched on 30 July 2025. The nominal duration of the mission is 3 years. The satellite carries onboard an L-band (24-cm wavelength) and an S-band (9.4-cm wavelength) radar with a swath width of approximately 240 km. Although NISAR supports various polarizations (single, dual, quad, circular), the SAR operates primarily in a dual-polarimetric mode with global acquisitions scheduled at L-band and targeted acquisitions schedules at S-band over the Indian subcontinent. The azimuth resolution is approximately 7–8 m. For the L-band radar, the range resolution varies between 3 m and 24 m, depending on the bandwidth, which ranges from 10 MHz to 75 MHz. Because of the wide swath, the incidence angle varies between 34 and 47 degrees. The NESZ is designed to be around –25 dB; the currently ongoing calibration phase of the mission will assess this level with observation data. At the time of writing, the mission is in its calibration/validation phase, and the first science data products have been released to the public.

NISAR flies with a 12-day repeat-pass orbit to allow interferometric observations and will acquire global imagery of Earth's land and ice on every cycle, producing on average around 35 Tb/day of data at L-band. NISAR data products are listed in Table 2. The Level-1 products are in the radar range-Doppler coordinate system. The Level-2 products are provided in map coordinate systems.

Table 2. Levels of the NISAR data products.

Product level	Product name
L0B	Raw data (public)
L1	Range-Doppler Single Look Complex (RSLC) Range-Doppler Wrapped Phase Interferogram (RIFG) Range-Doppler Unwrapped Interferogram (RUNW) Range-Doppler Pixel Offsets (ROFF).
L2	Geocoded SLC (GSLC) Geocoded Polarimetric Covariance (GCOV) Geocoded Unwrapped (GUNW) interferograms Geocoded Pixel Offsets (GOFF)

1.1. Purpose of document

This deliverable provides an overview of BIOMASS and NISAR signals, specifically for forests, and their potential for future retrieval of the above ground biomass (AGB, Mg or tonnes ha^{-1}). Given the novelty of the data streams provided by BIOMASS and NISAR, in this work we pursue two parallel studies.

1. Analyse the information content of BIOMASS and NISAR data (backscatter, InSAR, PolInSAR, TomoSAR) and test these in a biomass estimation framework, complementing retrievals at C- and L-band
2. Analyse the information content of BIOMASS and NISAR data products in an AGB post-processing framework (e.g., to bias-correct existing CCI BIOMASS maps)

Both pathways are explored to have a correct understanding of how BIOMASS and NISAR may contribute to wall-to-wall quantification of carbon stored in vegetation.

1.2. Contents

The document consists of the following sections:

- Section 2 outlines the downloading and pre-processing of NISAR and BIOMASS data as these have become available.
- Section 3 provides an initial analysis of NISAR and BIOMASS data for retrieving biomass variables, including *in situ* AGB and forest structure (e.g., height metrics from GEDI).
- Sections 4 outlines initial development of AGB retrievals from NISAR based on the CCI Biomass CORE algorithm.

2. Downloading and pre-processing of new sensor data

2.1. Study area and reference data

The study area presented in this section is situated to the southwest of the town of Mbalmayo, Cameroon. The reference AGB dataset was derived by integrating ground-based field inventory measurements (collected between April and July 2021) with Unmanned Aerial Vehicle (UAV) LiDAR data acquired in February 2023 over a 400-hectare extent (Rodda *et al.*, 2024). This open-access dataset is available through the IRD Dataverse repository [https://dataverse.ird.fr/] as a GeoTIFF file.

At a spatial resolution of 40 m, the reference product comprises three individual layers: the mean AGB and the standard deviation of AGB predictions, alongside a binning layer. For this analysis, the mean AGB layer was utilized. Figure 1 illustrates the spatial distribution of the mean AGB across the study site.

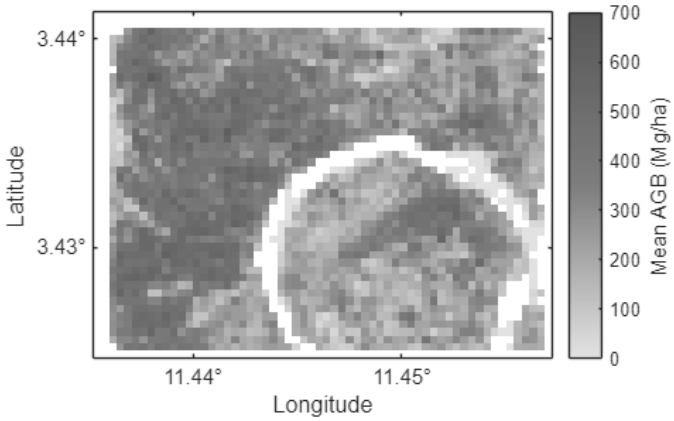

Figure 1. Map of the reference mean AGB for the Mbalmayo study site (40 m resolution) from Rodda et al. (2024). The colour gradient reflects aboveground biomass density (AGB) in Mg/ha, with water areas (the Nyong River) masked in white.

2.2. New sensor data

To ensure a robust and valid comparison, the SAR datasets were selected to provide full spatial overlap with the study area (Table 3). Furthermore, scenes from both the BIOMASS and NISAR sensors have an ascending orbit direction, and the temporal gap between their acquisitions is minimal. BIOMASS L1a and NISAR GCOV products were chosen for downloading and analysis because they can easily be converted to γ^0.

Table 3. List of regions and dates of acquisition for NISAR and BIOMASS

Sensor	Region	Date
NISAR	Mbalmayo, Cameroon	25 December 2025
BIOMASS	Mbalmayo, Cameroon	24 December 2025

2.3. NISAR

The NISAR Level-2 GCOV product for the study area was accessed through the Alaska Satellite Facility Distributed Active Archive Center (ASF DAAC) [https://asf.alaska.edu/]. The acquired dataset consists of L-band imagery with dual-polarization (HH and HV) capabilities. For this region, the Geocoded Polarimetric Covariance (GCOV) product provides terrain-flattened γ^0 backscatter values and terrain-corrected polarimetric covariance at a 20 m spatial resolution projected onto a predefined map projection [https://nisar-docs.asf.alaska.edu/gcov/]. The backscatter linear values were converted to a decibel (dB) scale using equation (1). Finally, the imagery was spatially subsetted using the bounding geometry of the reference dataset shapefile, and the HV band was selected for subsequent statistical analysis.

$$\gamma^0_{dB} = 10 \times \log_{10}(\gamma^0_{power}) \quad (1)$$

Figure 2 shows a map of the NISAR γ^0 L-HV image in dB and Figure 3 gives the corresponding histogram of pixel values. The very low backscatter values (in black in Figure 2, and shown as the low tail of the histogram in Figure 3) correspond to pixels over open water areas of the river.

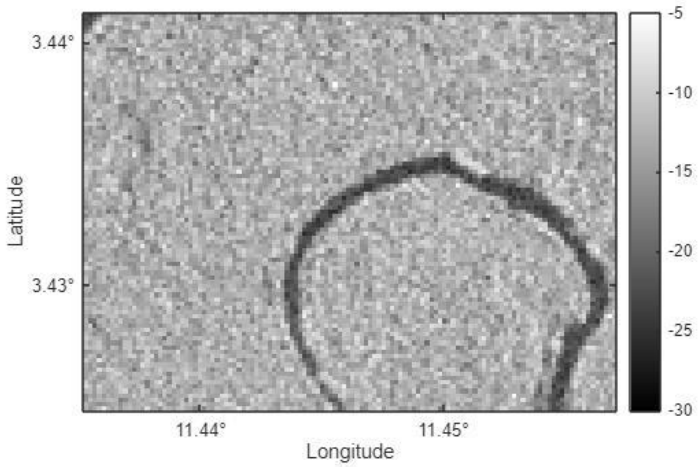

Figure 2. Spatially subsetted NISAR L-band γ^0 (dB) in HV channel over the reference study area.

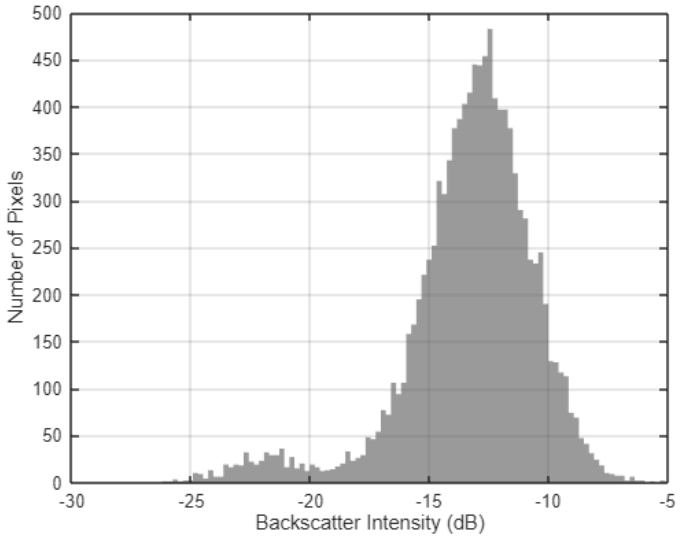

Figure 3. Histogram of NISAR L-band γ^0 HV backscatter (dB) for the study area.

2.4. BIOMASS

Pre-processing of the BIOMASS Level-1a SCS dataset, acquired via the ESA MAAP Explorer, was conducted using ESA's Sentinel Application Platform (SNAP, v13.0.1; Microwave Toolbox v13.0.3). The Level-1a product contains complex data records comprising amplitude and phase for each polarization.

The amplitude in BIOMASS Level-1a products represent the square root of beta-nought on a linear scale.

The first stage of the processing was radiometric calibration. This step mathematically squares the amplitude measurements at the pixel level to derive the beta-nought power values. Following radiometric calibration, a multilooking procedure was applied to the beta nought images to reducethe speckle noise and format the spatial scale for topographic correction. To ensure consistent geometry, a ground-range square pixel constraint was applied. The data was spatially averaged using one look in the range direction and six looks in the azimuth direction, generating a smoothed output with mean ground-range square pixels of approximately 40.45 m × 40.45 m. To further reduce the inherent speckle noise in the images, a filtering process was applied. The Lee Sigma filter was utilized using its default parameters in the ESA SNAP software: a base window size of 7x7, a target window size of 3x3, a sigma multiplier of 0.9, and the number of looks kept at 1.

To remove radiometric biases introduced by topographic variations, Radiometric Terrain Flattening was applied to the filtered beta-nought bands. This process converted the radar backscatter into terrain-flattened γ^0 values. The calculation utilized the auto-downloaded Copernicus 30m Global DEM with bilinear interpolation for resampling. As the 30m DEM possesses a higher spatial resolution than the ~40 m multilooked images, it successfully satisfied the algorithm's requirements using the default oversampling multiple of 1.0. Subsequently, to correct geometric distortions inherent to SAR viewing geometry caused by topographical variations, Range-Doppler Terrain Correction was applied. The terrain-flattened γ^0 bands were orthorectified and projected into the WGS84 geographic coordinate system. This geometric correction utilized the Copernicus 30m Global DEM, employing bilinear interpolation for both the DEM and the source image resampling. The final geocoded output maintained a pixel spacing of approximately 40.65 m, with areas lacking elevation data masked out.

Finally, the linear geocoded values were converted to a logarithmic decibel scale using the standard transformation (Equation 1). The processed BIOMASS imagery was spatially subsetted using the bounding geometry of the reference dataset shapefile, and the cross-polarized (HV) band selected for subsequent statistical analysis. Figure 4 shows the image subset and Figure 5 the corresponding histogram.

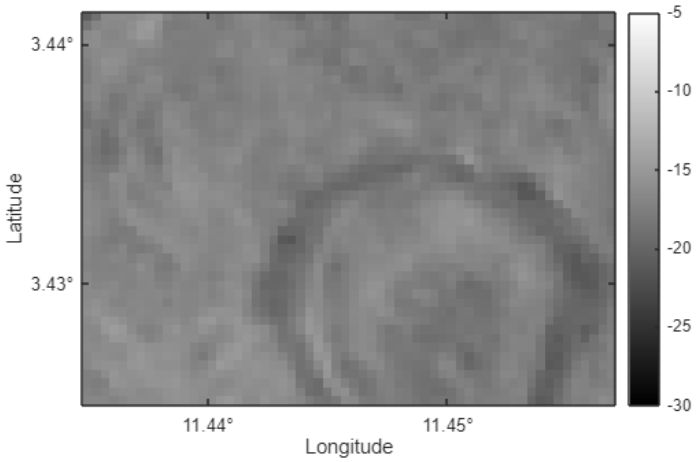

Figure 4. Spatially subsetted BIOMASS P-band γ^0 (dB) in HV channel over the reference study area after multi-looking and speckle filtering.

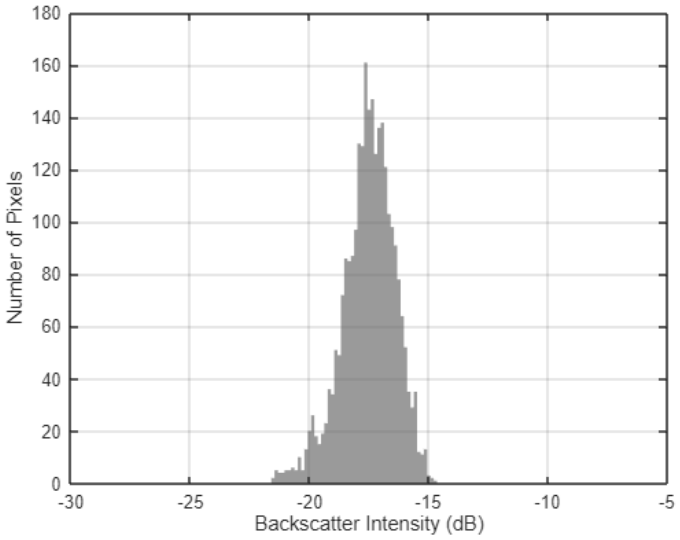

Figure 5. Histogram of BIOMASS P-band γ^0 HV backscatter (dB) for the study area.

2.5. Relationship Between Reference AGB and BIOMASS/NISAR Backscatter

To quantify the relationship between SAR backscatter and AGB, the BIOMASS and NISAR γ^0 intensity images were first spatially interpolated to match the 40 m resolution grid of the reference AGB dataset. Following the framework described by Pulliainen et al. (1996), the relationship was modelled using an exponential equation where the total forest backscatter (γ^0) in a linear scale is a function of biomass (Vol):

$$\gamma^0 = a - e^{-(b.Vol+c)} \quad (2)$$

where a represents the backscatter saturation level, b defines the shape of the fitted curve, and c relates to the target's backscatter at zero biomass compared to the saturation level. The model was fitted to the dataset using non-linear least squares regression applied to the linear power intensities. To better visualize the backscatter trends, the raw pixel data was aggregated into discrete AGB bins of 50 Mg/ha width (representing intervals of ±25 Mg/ha around the centre of the bin). Within each bin, the mean γ^0 backscatter coefficient and its corresponding standard deviation were calculated.

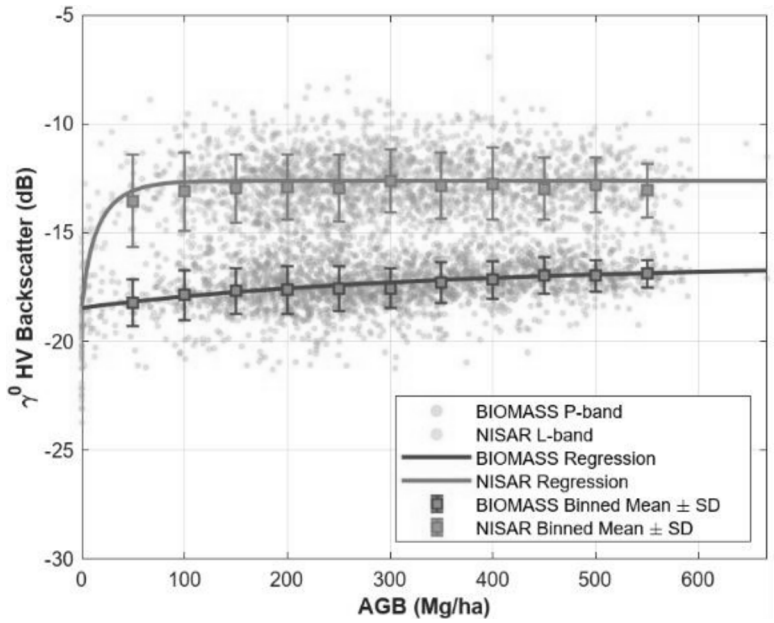

Figure 6. Comparison of BIOMASS and NISAR γ^0 HV backscatter against reference AGB. Solid lines represent the fitted exponential saturation models, with square markers indicating the mean and standard deviation derived from a 50 Mg/ha AGB interval binning.

Figure 6 plots the P-band and L-band γ^0 backscatter at 40 m spatial resolution against reference AGB. The fitted regression curves for both wavelengths show similar overall trends with respect to increasing AGB. The L-band backscatter demonstrates high sensitivity to AGB up to about 100 Mg/ha, after which this sensitivity begins to decline as the signal approaches saturation. While the P-band signal sensitivity extends to much higher AGB values, its overall dynamic range from low to high biomass is significantly smaller compared to that of the L-band.

3. Initial analysis for AGB estimation

Existing space-based SAR sensors penetrate forest canopy to different depths, with the C-band limited to the upper canopy and the L-Band reaching deeper branches (Imhoff, 1995; Le Toan *et al.*, 2011). BIOMASS's P-band offers the possibility to reach deeper under-canopy structures, notably trunks and understoreys, and is thus expected to saturate at higher levels of aboveground biomass than the C-band and L-band.

In the below analysis, we:

1) Provide a preliminary analysis of NISAR and BIOMASS sensitivity to canopy height and high biomass, in comparison with existing spaceborne SAR observations (ALOS PALSAR 2 L-band and Sentinel 1 C-band) using AGB derived from airborne LiDAR data acquired at site level

2) Explore BIOMASS Level 2A product across AGB amounts and terrain steepness at landscape scale.

3.1. NISAR and BIOMASS saturation at high biomass

To compare their saturation threshold with existing spaceborne SAR observations, we used Sentinel-1's C-band from Ground Range Detected (GRD) product (Copernicus & European Space Agency, 2015) [https://developers.google.com/earth-engine/datasets/catalog/COPERNICUS_S1_GRD] and ALOS-2 PALSAR-2's L-band from the yearly mosaic version 2.5.0 (Shimada *et al*, 2014) [https://developers.google.com/earth-engine/datasets/catalog/JAXA_ALOS_PALSAR_YEARLY_SAR_EPOCH]. To avoid anomalous observations, we averaged all the images acquired by these instruments starting from 2023 up to now. PALSAR pixel values were converted to decibels following the formula for $\gamma_0 = 10\log_{10}(DN^2) - 83.0$ dB. Sentinel-1 data were already provided on a dB scale.

BIOMASS and NISAR data were extracted and calibrated as described in Section 2. Ground truth AGB measurements were obtained from airborne LiDAR and field observations in Cameroon, as detailed in Section 2 (Rodda *et al.* 2024). The site selected presents high AGB densities (maximum = 419 $t.ha^{-1}$, mean = 257.18 $t.ha^{-1}$ at 100m spatial resolution). We reclassified the AGB values into bins to calculate backscatter statistics with reduced dispersion and thereby better detect patterns across the AGB gradient. Due to the limited number of pixels in the site (415 usable pixels at 100m spatial resolution), we used intervals of 100 $t.ha^{-1}$ to maximise the number of pixels per bin and better reduce noise. To explore SAR backscatter behaviour across canopy height, we also used a Canopy Height Model derived from GEDI and Landsat measurements for year 2019 (Potapov *et al.*, 2019) [https://glad.earthengine.app/view/global-forest-canopy-height-2019].

Figure 7 shows a scatterplot of radar backscatter coefficient in dB from different sensors against AGB in $t.ha^{-1}$, indicating that the P-band backscatter does not saturate for high AGB values, unlike the L-band and C-band.

Figure 8 shows radar backscatter coefficient plotted against canopy height in metres. It shows a more linear relationship between the P-band backscatter and canopy height that does not exhibit any sign of saturation, unlike the L-band and C-band backscatter curves.

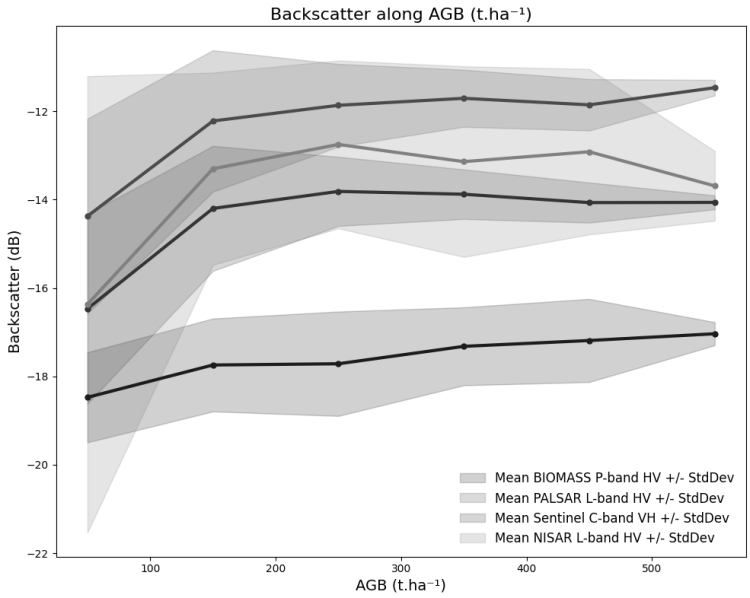

Figure 7. PALSAR-2, Sentinel-1 and NISAR tend to saturate above approximately 150 t.ha^{-1} of AGB, while BIOMASS P-band SAR continues to increase linearly, indicating its continued sensitivity to higher biomass. NISAR shows high levels of noise, likely due to some unresolved calibration issues.

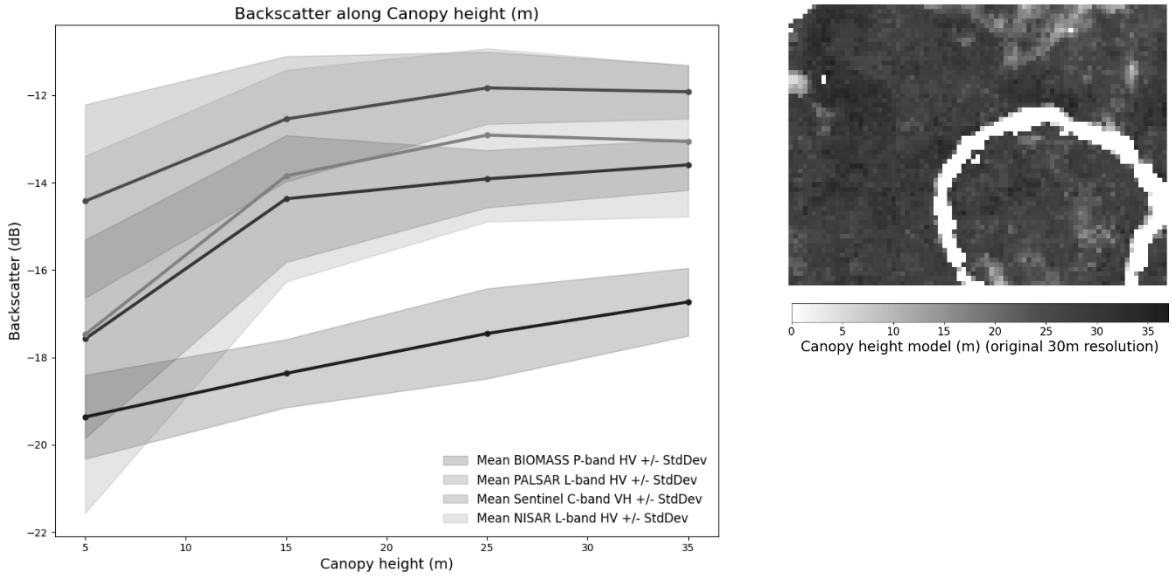

Figure 8. The patterns are more pronounced when plotting radar backscatter coefficient in dB against canopy height in metres (processed at 100m resolution). Both PALSAR and NISAR L-bands become less sensitive to canopy height increase at around 25 m, while Sentinel-1 C-band starts to saturate in lower stature (10-15 m) forests and woodlands. The P-band backscatter remains linearly related to canopy height across the range.

3.2. BIOMASS Level 2A

We analysed the first (and only) Level 2A (FP_GN__L2A) image that was made available in the MAAP catalogue, as of 19th March 2026 [https://explorer.maap.eo.esa.int/]. The image is in GeoTiff format and consists of 3 bands, each representing a polarisation (HH, VH and VV respectively). The Ground Notched product contains ground cancelled calibrated backscatter derived from the Level 1C and auxiliary data [https://earth.esa.int/eogateway/documents/d/earth-online/biomass-forest-height-products-format-specification]. Pixel values represent sigma-nought expressed on a linear scale. To convert these to decibels, we used the below formula:

$$\sigma^0_{dB} = 10\, log_{10}(\sigma^0_{power})$$

We did not apply any further correction (i.e., for geometric effects etc.).

The BIOMASS SAR images were acquired between 6th and 10th October 2025 in South America and covered landscapes spanning Paraguay and the State of Mato Grosso Do Sul in Brazil (Figure 9). The landscape consists of a mosaic of agricultural lands and fragmented woodlands and rangelands as discerned from canopy height estimations from GEDI and Landsat in 2019 (Figure 10, right map) and the latest Landsat-based land cover map available, extracted from the Global 30-meter Land Cover Change Dataset (GLC FCS, Figure 10, left map) and which covers the year 2022 (Zhang et al, 2024).

As ground AGB measurements for this area are not available, AGB estimates were extracted from version 7 of the ESA CCI AGB product for the year 2024, which is the closest to the year of BIOMASS acquisitions (i.e. 2025). After masking non-treed/non-woody land covers, the landscape presents relatively low AGB estimates (maximum = 165 t.ha^{-1}, mean = 37.97 t.ha^{-1}). The AGB map was reclassified into bins representing 10 t.ha^{-1} intervals. The mean and standard deviation of the SAR backscatter were then calculated for the three instruments by AGB bin at 100 m resolution. The VH band of Sentinel C-band SAR and the HV band of PALSAR L-band SAR were compared with the BIOMASS P-band HV data. Focus was on the cross-polarisations (VH and HV) data because these often show greater correlation with AGB, compared to the co-polarised data (HH and VV) (Rodriguez-Veiga et al, 2025). The resulting scatterplot of BIOMASS P-band SAR backscatter against AGB is shown in Figure 11.

The effects of topography on the P-band were also explored using a Digital Elevation Model (DEM) extracted from ALOS World 3D - 30m version 4.1 (Tadono et al, 2014) [https://developers.google.com/earth-engine/datasets/catalog/JAXA_ALOS_AW3D30_V4_1]. Slope was derived from the DEM in degrees (0 = horizontal, 90 = vertical) and reclassified it into bins of 1 degree interval (Figure 12). However, vegetation canopies are not sufficiently tall/dense in this landscape, which limits our ability to interpret backscatter relationship with forests.

Figure 13 indicates that the backscatter from Sentinel-1, ALOS-2 and BIOMASS is heavily influenced by steep slopes over about 25 degrees. We recommend that these should be masked out when creating AGB maps from SAR.

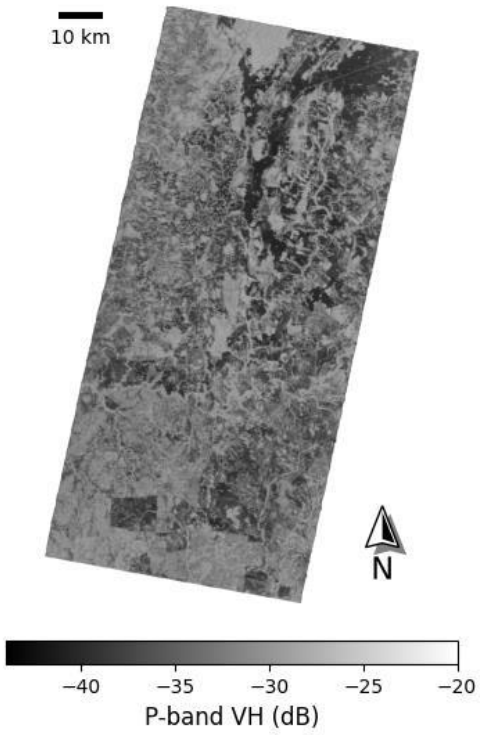

Figure 9. BIOMASS SAR P-band VH image over the study site (File name bio_fp_gn__l2a_20251006t214648_20251021t214702_c_g___m___c___t____f174_i_gn)

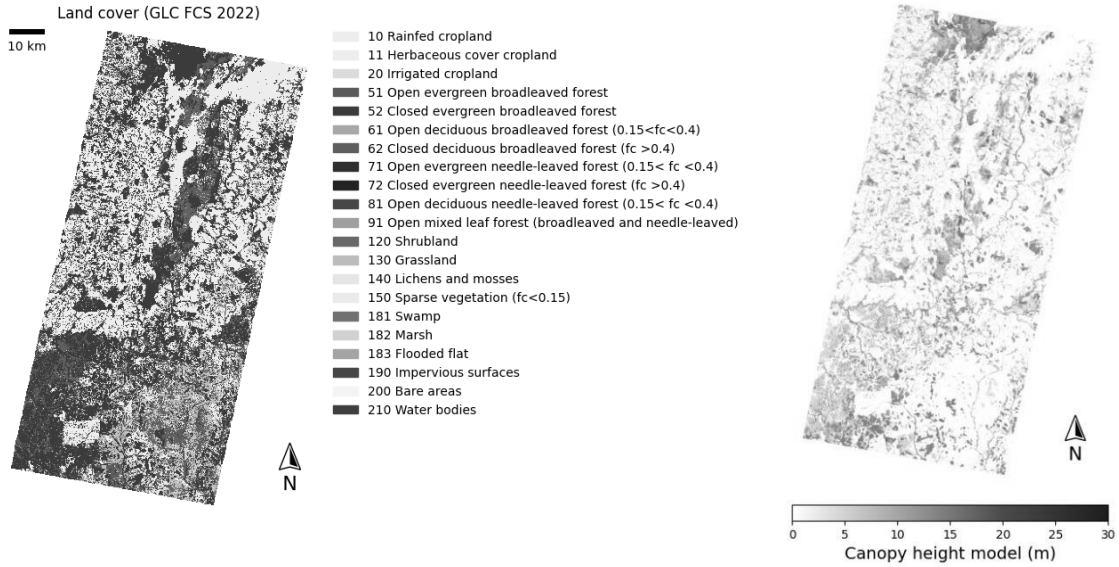

Figure 10. Land cover map (2022) (left) and canopy height model (2019) (right) over the study site.

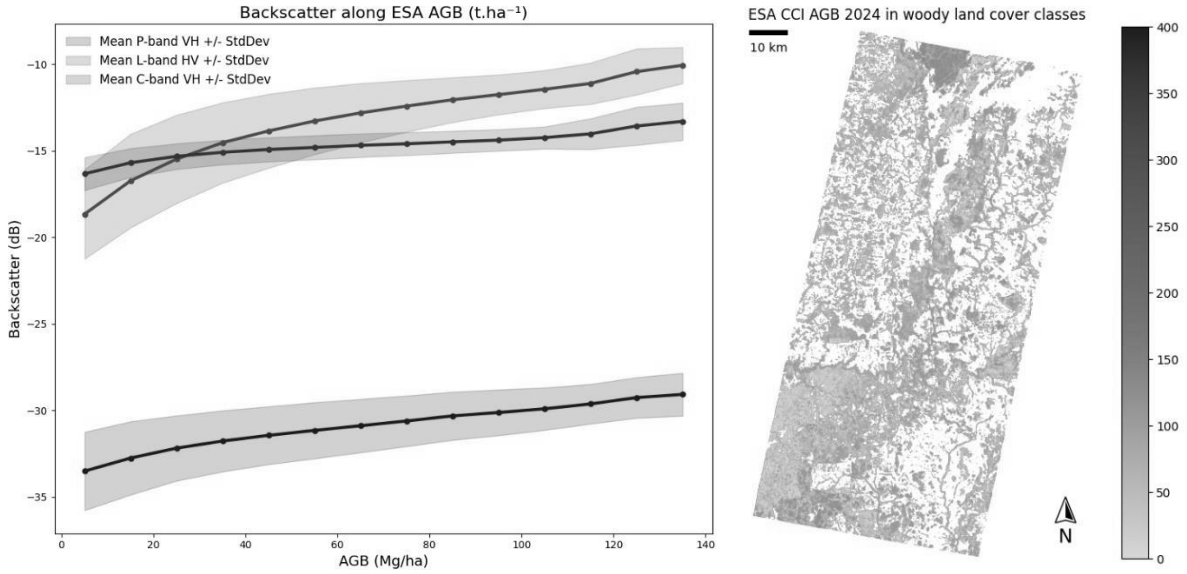

Figure 11. SAR cross-polarisation comparison across AGB from ESA CCI 2024 (t.ha^{-1}) over the study site for C-, L- and P-band from Sentinel-1, ALOS-2 and BIOMASS (ground cancelled).

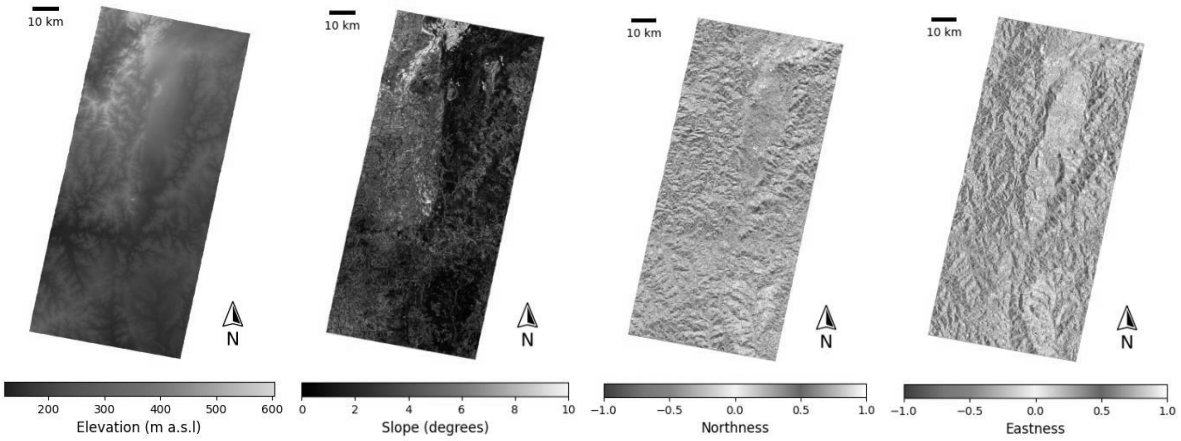

Figure 12. Terrain variables derived from the ALOS World 3D DEM.

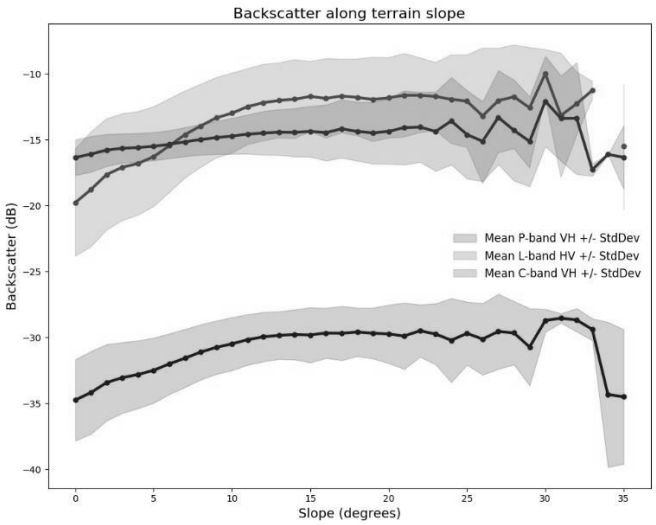

Figure 13. Relationship with terrain slope (higher variability at steeper slopes are due to the smaller numbers of pixels per bin). The P-band backscatter has been ground cancelled.

4. AGB retrieval based on the CCI Biomass Core Algorithm

NISAR data are in principle comparable to those generated by the ALOS series of satellites and may therefore be ingested in the BIOMASAR-L component of the CCI Biomass CORE retrieval algorithm as they are. For each L-band image, BIOMASAR-L estimates the two unknown parameters of a Water Cloud Model, i.e., the backscatter coefficients of an unvegetated surface and of an ideally opaque vegetation layer and inverts the Water Cloud Model to obtain an estimate of AGB for a measurement of the SAR backscatter. BIOMASAR-L operates without the need of ground reference measurements of AGB to be able to represent the relationship between the backscatter and the AGB everywhere. For details on how the calibration of BIOMASAR-L is performed, refer to the Algorithm Theoretical Basis Document (ATBD) of the CCI Biomass project [RD-1]. In the case of NISAR, each pixel is characterized by multiple observations of SAR backscatter during one year so that a final estimate of AGB is then obtained by applying a weighted linear average of the individual AGB estimates. The weights correspond to the difference of the two backscattering coefficients for the opaque canopy and the unvegetated terrain.

Given the very recent availability of a first batch of NISAR data, it has not been possible to test BIOMASAR-L with such data in time for the submission of this report. The NISAR data will be evaluated during the next reporting phase and results presented in the next version of this report due March 2027.

5. References

Araza, A., de Bruin, S., Herold, M., Quegan, S., Labriere, N., Rodriguez-Veiga, P., Avitabile, V., Santoro, M., Mitchard, E.T.A., Ryan, C.M., Phillips, O.L., Willcock, S., Verbeeck, H., Carreiras, J., Hein, L., Schelhaas, M.-J., Pacheco-Pascagaza, A.M., da Conceição Bispo, P., Laurin, G.V., Vieilledent, G., Slik, F., Wijaya, A., Lewis, S.L., Morel, A., Liang, J., Sukhdeo, H., Schepaschenko, D., Cavlovic, J., Gilani, H., Lucas, R., 2022. A comprehensive framework for assessing the accuracy and uncertainty of global above-ground biomass maps. *Remote Sensing of Environment* 272, 112917. https://doi.org/10.1016/j.rse.2022.112917

Copernicus & European Space Agency. 2015. Sentinel-1 SAR GRD: C-band Synthetic Aperture Radar Ground Range Detected, log scaling. Available in Google Earth Engine. https://developers.google.com/earth-engine/datasets/catalog/COPERNICUS_S1_GRDImhoff, M.L., 1995. A theoretical analysis of the effect of forest structure on synthetic aperture radar backscatter and the remote sensing of biomass. *IEEE Transactions on Geoscience and Remote Sensing*, 33(2), pp.341-351.

Le Toan, T., Quegan, S., Davidson, M.W.J., Balzter, H., Paillou, P., Papathanassiou, K., Plummer, S., Rocca, F., Saatchi, S., Shugart, H. and Ulander, L., 2011. The BIOMASS mission: Mapping global forest biomass to better understand the terrestrial carbon cycle. *Remote Sensing of Environment*, 115(11), 2850-2860.

Kellogg, K., Hoffman, P., Standley, S., Shaffer, S., Rosen, P., Edelstein, W., Dunn, C., Baker, C., Barela, P., Shen, Y. & Guerrero, A.M. 2020. March. NASA-ISRO synthetic aperture radar (NISAR) mission. In *2020 IEEE aerospace conference* (pp. 1-21). IEEE. Quegan, S., Le Toan, T., Chave, J., Dall, J., Exbrayat, J.-F., Minh, D.H.T., Lomas, M., D'Alessandro, M.M., Paillou, P., Papathanassiou, K., Rocca, F., Saatchi, S., Scipal, K., Shugart, H., Smallman, T.L., Soja, M.J., Tebaldini, S., Ulander, L., Villard, L., Williams, M., 2019. The European Space Agency BIOMASS mission: Measuring forest above-ground biomass from space. *Remote Sensing of Environment* 227, 44–60. https://doi.org/10.1016/j.rse.2019.03.032

Potapov, P., Li, X., Hernandez-Serna, A., Tyukavina, A., Hansen, M. C., Kommareddy, A., Pickens, A., Turubanova, S., Tang, H., Silva, C. E., Armston, J., Dubayah, R., Blair, J. B., & Hofton, M. 2021. Mapping global forest canopy height through integration of GEDI and Landsat data. *Remote Sensing of Environment*, 253. https://doi.org/10.1016/j.rse.2020.112165

Pulliainen, J.T., Mikkelä, P.J., Hallikainen, M.T. and Ikonen, J.P., 1996. Seasonal dynamics of C-band backscatter of boreal forests with applications to biomass and soil moisture estimation. *IEEE Transactions on Geoscience and Remote Sensing*, 34(3), 758-770.

Rodda, S.R., Fararoda, R., Gopalakrishnan, R. et al. 2024. LiDAR-based reference aboveground biomass maps for tropical forests of South Asia and Central Africa. *Sci Data* 11, 334. https://doi.org/10.1038/s41597-024-03162-x

Rodda, SR et al. 2024. South Asian and Central African maps from: LiDAR-based reference aboveground biomass maps for tropical forests of South Asia and Central Africa. *Dataverse*. DataSuds, V2, UNF:6:pUYwyUIpsRWmCnpBju2KxQ== [fileUNF] https://doi.org/10.23708/H2MHXF

Rodríguez-Veiga, P., Carreiras, J.M.B., Quegan, S. et al. 2025. Loss of tropical moist broadleaf forest has turned Africa's forests from a carbon sink into a source. *Sci Rep* 15, 41744. https://doi.org/10.1038/s41598-025-27462-3

Rosen, P.A., Bawden, G.W., Barela, P., Chapman, B., Fattahi, H., Jones, C.E., Joughin, I.R., Lavalle, M., Lohman, R.B., Simons, M., Siqueira, P., Das, A., Desai, N.M., Kumar, R., Putrevu, D., Sharma, R., Shrikant, C., 2025. The NASA-ISRO SAR Mission: A summary. *IEEE Geosci. Remote Sens. Mag*. 13, 8–34. https://doi.org/10.1109/MGRS.2025.3578258

Shimada M, Itoh T, Motooka T, Watanabe M, Tomohiro S, Thapa R, & Lucas R. 2014. New Global Forest/Non-forest Maps from ALOS PALSAR Data (2007-2010). *Remote Sensing of Environment*, 155, 13-31. https://doi.org/10.1016/j.rse.2014.04.014 T.

Tadono, H. Ishida, F. Oda, S. Naito, K. Minakawa & H. Iwamoto. 2014. Precise Global DEM Generation By ALOS PRISM, *ISPRS Annals of the Photogrammetry, Remote Sensing and Spatial Information Sciences*, II-4, 71-76

Zhang, X., Zhao, T., Xu, H., Liu, W., Wang, J., Chen, X., and Liu, L. 2024. GLC_FCS30D: the first global 30 m land-cover dynamics monitoring product with a fine classification system for the period from 1985 to 2022 generated using dense-time-series Landsat imagery and the continuous change-detection method, *Earth Syst. Sci*. Data, 16, 1353–1381, https://doi.org/10.5194/essd-16-1353-2024